SYNTHETIC APERTURE IMAGING USING A LAGRANGE BASED FILTERING TECHNIQUE

Pai-Chi Li and M. O'Donnell

Electrical Engineering and Computer Science Department
University of Michigan
Ann Arbor, MI 48109-2122

Synthetic aperture imaging using a catheter based, circular phased array providing high resolution, dynamic focusing has been explored. Due to the high input impedance and low signal-to-noise ratio (SNR) of a classic single element synthetic aperture system, multi-element synthetic aperture processing has been proposed with SNR improvement of about 8 dB for a 33 element aperture. Reconstruction in this case uses an optimal filtering approach based on minimizing the mean square error between filter output and desired beam pattern. This approach, however, does not directly control both mainlobe beamwidth and sidelobe levels. To overcome this problem, a Lagrange based filter design technique has been developed that not only satisfies the minimum energy criterion, but also constrains sidelobe levels under a certain threshold. The new technique provides better spatial and contrast resolution. Both the mathematical formulation and simulation results are presented. © 1992 Academic Press, Inc.

Key words: Catheter-based imaging; circular array: Lagrange multiplier; medical ultrasound; synthetic aperture.

1 INTRODUCTION

Catheter based, circular phased arrays have been investigated and developed as a diagnostic tool for coronary artery disease. The operating frequency and aperture size of ultrasonic intravascular imagers is basically determined by a tradeoff between depth of field and resolution [1-8]. In addition, the degree of control over dynamic beam forming is constrained by the requirement of minimal electrical interconnection to the array at the catheter tip. Consequently, high resolution, dynamic beam forming over a large depth of field with minimal interconnection requires some form of synthetic aperture processing of catheter array data.

In a classic synthetic aperture imaging system, a single element of the circular array is used as both transmitter and receiver on each firing. Due to the geometry of the circular array, the output of a particular beam direction is the coherent sum over a set of elements satisfying an acceptance criterion on the propagation angle. The time delay for each individual element in the coherent sum is determined by both the normal focus delay and the circular geometry [9]. Note that the received radio frequency (rf) signal can be baseband demodulated using a simple digital baseband circuit [10]. By assuming the time delay does not vary dramatically over the pulse envelope function, synthetic aperture reconstruction can be expressed as

$$O_n(t) = \sum_{n-M}^{n+M} b_k(t)\left[\frac{e^{jw_0\tau_k}}{a(\phi_k)/R_k'^2}\right] \qquad (1)$$
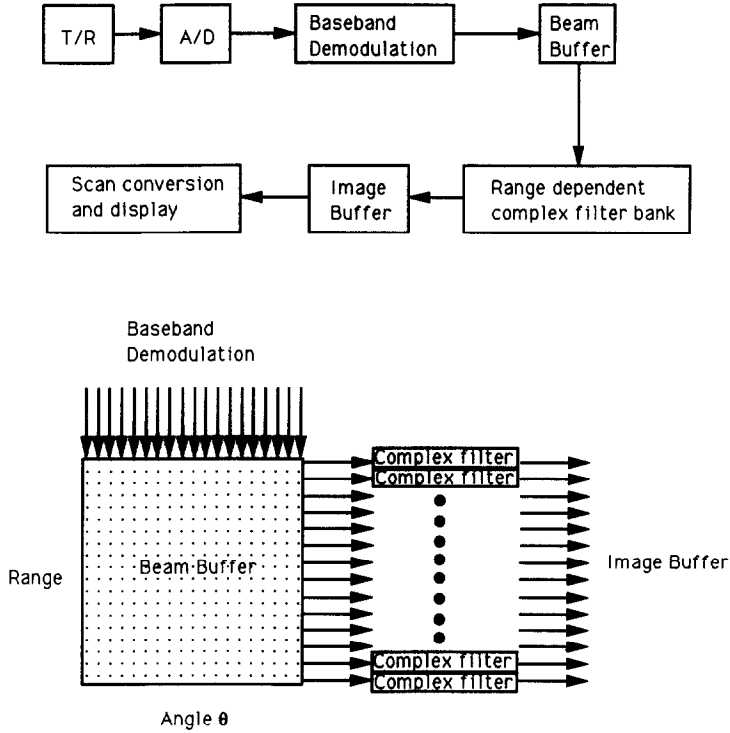
Fig. 1 Block diagram for range dependent, complex filtering.

where $O_n(t)$ is the complex baseband output formed by the coherent sum of $2M + 1$ firings representing the imaging aperture and M is determined by a minimum f/number criterion. The complex baseband signal from the kth element, $b_k(t)$, is weighted by $\frac{e^{jw_0\tau_k}}{a(\phi_k)/R_k'^2}$, where w_0 is the angular carrier frequency, $a(\phi_k)$ is the kth element's angular response and τ_k, R_k' are the propagation time and distance from the kth element to the reconstructed point respectively [9]. As shown in Eq.(1), reconstruction is simply a range dependent complex filtering operation on the baseband signal for each firing.

The basic block diagram for performing this type of complex filtering operation is shown in figure 1. Note that a pipeline structure is used for these range-dependent filters and the complex filter coefficients are pre-calculated and stored in the filter bank. Hence, this architecture is suitable for real time application.

Although producing spatial and contrast resolution comparable to a full phased array system, a single element synthetic aperture imaging system produces images with low electronic signal to noise ratio (SNR). The SNR is low, first, because the electrical impedance of each individual element is very high, and second, because the acoustic power delivered to the body is very small. At very high frequencies, SNR losses make this kind of imaging system impractical.

An alternative synthetic aperture system using n ($n \geq 2$) elements in the array as the transceiver on each given firing can greatly improve the SNR. For this system, the

electrical impedance becomes $\frac{1}{n}$ of the single element impedance and approximately n times the acoustic power is delivered for the same drive voltage. SNR improvements are gained, however, at the expense of beam quality. It is possible, however, to use complex filtering to compensate for degradation of a synthetic focus. As described in reference [9], the overall SNR improvement can be defined as

$$SNR(dB) = 10\log_{10} \frac{|filtered|^2}{|single\ element|^2 \sum_{-M}^{M} |F_i|^2} \qquad (2)$$

where $|filtered|$ stands for the magnitude of the filter output, $|single\ element|$ represents the magnitude of the unfiltered single element signal and $|F_i|$ is the magnitude of the ith filter coefficient. Note that for the complex filtering operations described here, the details of the filter coefficients can affect the overall SNR of the system.

As noted above, synthetic aperture reconstruction is basically a complex filtering operation [9]. One optimal approach to this problem is to minimize the mean square error between the desired beam pattern and the filter output. In other words, let $d(i)$ represent the ith sample of the desired beam pattern, $b(i)$ be the complex baseband sample from the ith firing of the array and $f(i)$ stand for the ith optimal filter coefficient; the mean square error can be defined as

$$\varepsilon = \sum_{n} w(n)[d(n) - \sum_{k=n-M}^{n+M} b(k)f(k-n)]^2 \qquad (3)$$

where the complex filter has $2M+1$ lags and $w(n)$ is the weighting term defined as

$$w(n) = \begin{cases} \frac{1}{d(n)^2} & |d(n)| \geq \gamma \\ \frac{1}{\gamma^2} & \text{otherwise} \end{cases} \qquad (4)$$

where γ is chosen to avoid numerical instability. By setting the partial derivative of ε with respect to both real and imaginary parts of the filter coefficients to zero, the optimal filter can be obtained. Since this minimizes total error, overall image quality is greatly improved as shown in reference [9].

Over all imaging ranges in the far field of an individual sub-aperture (i.e., n elements), the multi-element system is a great improvement over classic synthetic aperture processing. Nevertheless, this approach can provide relatively high peak sidelobe levels since only the error energy is minimized. Also, the mainlobe beamwidth in this case is not independently controllable. That is, we do not have simultaneous control over both resolution and peak sidelobe levels.

Recently, a new optimal window design algorithm has been proposed [11]. This frequency domain window defines optimality by an efficient tradeoff between the least-squares solutions, e.g., prolate-spheroidal windows, and minimax solutions, e.g., Chebyshev windows. Briefly, this efficient tradeoff is achieved by introducing a quadratic programming problem with linear constraints. As such, it can be solved using Lagrange multipliers.

We note that the frequency domain optimal window design problem is equivalent to the space domain filter design problem in some senses. First, to increase resolution, the space domain mainlobe beamwidth should be reduced. On the other hand, sidelobe levels should be kept under some acceptable threshold. These criteria can be viewed as the minimax condition in the window design problem. Second, improving SNR is equivalent to the least square criterion in the window design problem. One of the main differences between these two problems, however, is that the mainlobe beamwidth and sidelobe level are defined in the frequency domain in the window design problem, while in the synthetic

aperture problem they are defined in the space domain. This Lagrange based technique has also been applied to coded excitation systems [12].

In the following section, we will present a formal statement of the problem. Some simulation results will be shown in section 3, and the results are discussed in section 4.

2   A LAGRANGE BASED FILTERING TECHNIQUE

Within the region of interest of the circular array, the range is divided into several focal zones. The goal of this design problem is to choose an independent complex filter, $\mathbf{f}$, for each zone such that after application of this filter to the discrete baseband signal $\mathbf{b}$, the resultant output $\mathbf{y}$ satisfies certain design criteria, i.e., mainlobe beamwidth and sidelobe level δ specified in dB. Note that due to the array geometry, the filtering operation is performed as a circular convolution. Let the discrete signals $\mathbf{b}$ and $\mathbf{f}$ be defined as

$$\mathbf{b} \stackrel{\text{def}}{=} [b(0), \ldots, b(n-1)]^t$$

$$\mathbf{f} \stackrel{\text{def}}{=} [f(-M), \ldots, f(M)]^t \qquad ,$$

then $\mathbf{y} = \mathbf{b} \circledast \mathbf{f}$ where $\circledast$ stands for circular convolution, and this convolution can be represented in matrix form as

$$\mathbf{y} = \mathbf{Bf} \qquad , \tag{5}$$

where

$$\mathbf{B} \stackrel{\text{def}}{=} \begin{pmatrix} b(n-M) & b(n-M+1) & b(n-M+2) & \cdots & b(M) \\ b(n-M+1) & b(n-M+2) & b(n-M+3) & \cdots & b(M+1) \\ \vdots & \vdots & \vdots & \vdots & \vdots \\ b(0) & b(1) & \cdots & \cdots & b(2M) \\ \vdots & \vdots & \vdots & \vdots & \vdots \\ b(n-M-1) & b(n-M) & \cdots & \cdots & b(M-1) \end{pmatrix} \tag{6}$$

For convolution processing, sidelobe energy can be represented by

$$\varepsilon \stackrel{\text{def}}{=} \sum_{i \in \text{sidelobe region}} |y_i|^2 = \mathbf{y}^\mathbf{H} \mathbf{A} \mathbf{y} \qquad , \tag{7}$$

where $\mathbf{y}^\mathbf{H}$ stands for $\mathbf{y}$'s Hermitian conjugate and $\mathbf{A}$ is defined as

$$\mathbf{A} \stackrel{\text{def}}{=} \begin{pmatrix} 1 & & & & & & & \\ & \ddots & & & & & \bigcirc & \\ & & 1 & & & & & \\ & & & 0 & & & & \\ & & & & \ddots & & & \\ & & & & & 0 & & \\ & & & & & & 1 & \\ & \bigcirc & & & & & & \ddots & \\ & & & & & & & & 1 \end{pmatrix} \tag{8}$$

i.e., $\mathbf{A}$ is a square matrix of dimension n with all zero elements except along the diagonal in the sidelobe region.

Using Eqs. (5)-(8) the sidelobe energy can be expressed as

$$\varepsilon \stackrel{\text{def}}{=} \sum_{i \in \text{sidelobe region}} |y_i|^2 = \mathbf{y}^{\mathbf{H}}\mathbf{A}\mathbf{y} = \mathbf{f}^{\mathbf{H}}\mathbf{B}^{\mathbf{H}}\mathbf{A}\mathbf{B}\mathbf{f} \tag{9}$$

If we define a new matrix $\mathbf{Q}$ as

$$\mathbf{Q} \stackrel{\text{def}}{=} \mathbf{B}^{\mathbf{H}}\mathbf{A}\mathbf{B}$$

then the energy becomes

$$\varepsilon \stackrel{\text{def}}{=} \mathbf{f}^{\mathbf{H}}\mathbf{Q}\mathbf{f} \tag{10}$$

where $\mathbf{Q}$ is an $2M + 1 \times 2M + 1$ Hermitian matrix, i.e., $\mathbf{Q} = \mathbf{Q}^{\mathbf{H}}$

To constrain peak-sidelobe levels, a set of control points in the sidelobe region is prespecified. All control points are forced to have amplitude equal to or less than δ. Consequently, these linear constraints can also be represented in matrix form as

$$\mathbf{C}\mathbf{f} = \mathbf{c} \tag{11}$$

where l is the number of control points and $\mathbf{C}$ is an $l \times 2M + 1$ matrix performing circular convolution on the control points. On the other hand, the magnitude of each element in $\mathbf{c}$ is simply δ expressed as a fraction of the overall filter gain. Since both the baseband signal and the filter are complex, however, $\mathbf{c}$ is also complex. Therefore, choosing the optimal phase for $\mathbf{c}$ is an important issue, as discussed below.

So far, the problem can be stated as follows:

Given baseband signal $\mathbf{b}$, *choose* $\mathbf{f}$ *to minimize* $\varepsilon \stackrel{\text{def}}{=} \mathbf{f}^{\mathbf{H}}\mathbf{Q}\mathbf{f}$ *subject to* $\mathbf{C}\mathbf{f} = \mathbf{c}$.

As demonstrated in [11], a simple Lagrangian function Λ representing a linear combination of the energy and constraint equations, i.e.,

$$\Lambda(\mathbf{f}, \lambda) \stackrel{\text{def}}{=} \mathbf{f}^{\mathbf{H}}\mathbf{Q}\mathbf{f} - \lambda^{\mathbf{H}}(\mathbf{C}\mathbf{f} - \mathbf{c}) \tag{12}$$

can be used to determine optimal filter coefficients. It can be easily shown that the optimal solution to Eq. (12) given that $\mathbf{Q}$ is non-singular is

$$\mathbf{f} = \mathbf{Q}^{-1}\mathbf{C}^{\mathbf{H}}[\mathbf{C}\mathbf{Q}^{-1}\mathbf{C}^{\mathbf{H}}]^{-1}\mathbf{c} \tag{13}$$

This is the weighted minimum norm solution, which also can be obtained using projection theory. In other words, if the inner product space is defined as $< \mathbf{x}, \mathbf{y} >_{\mathbf{Q}} = \mathbf{x}^{\mathbf{H}}\mathbf{Q}\mathbf{y}$, it can be shown that the Lagrange multiplier solution is equivalent to the minimum-norm solution under that inner product space.

As noted above, choice of the phases in $\mathbf{c}$ is arbitrary. Since one of the design goals is to maximize the contrast between the energy in mainlobe and sidelobes, where a quantitative measure of this constraint is defined as

$$CR(\text{contrast ratio}) \stackrel{\text{def}}{=} \frac{\text{total energy}}{\text{sidelobe energy}} = \frac{\mathbf{y}^{\mathbf{H}}\mathbf{y}}{\mathbf{y}^{\mathbf{H}}\mathbf{A}\mathbf{y}} \tag{14}$$

the set of optimal phases at the control points should maximize this CR.

According to Eq. (13) and defining

$$\mathbf{X} \stackrel{\text{def}}{=} \mathbf{B}\mathbf{Q}^{-1}\mathbf{C}^{\mathbf{H}}[\mathbf{C}\mathbf{Q}^{-1}\mathbf{C}^{\mathbf{H}}]^{-1} \tag{15}$$

eq. (14) can be rewritten as

$$CR \stackrel{\text{def}}{=} \frac{\mathbf{c}^H \mathbf{X}^H \mathbf{X} \mathbf{c}}{\mathbf{c}^H [\mathbf{C} \mathbf{Q}^{-1} \mathbf{C}^H]^{-1} \mathbf{c}} \qquad (16)$$

Finally, defining

$$\mathbf{c}' \stackrel{\text{def}}{=} [\mathbf{X}^H \mathbf{X}]^{1/2} \mathbf{c} \stackrel{\text{def}}{=} \mathbf{U} \mathbf{c}$$

and

$$\mathbf{D} \stackrel{\text{def}}{=} [\mathbf{U} \mathbf{C} \mathbf{Q}^{-1} \mathbf{C}^H \mathbf{U}^H]^{-1}$$

the CR can be simply expressed as:

$$CR = \frac{\mathbf{c}'^H \mathbf{c}'}{\mathbf{c}'^H \mathbf{D} \mathbf{c}'} \qquad (17)$$

Determining the phases in Eq. (17) is equivalent to the eigenvalue problem described in [13]. This technique starts by expressing CR as a function of $\mathbf{c}'$. Setting $\delta CR = 0$ with respect to $\mathbf{c}'$, it can be shown that the maximum CR is obtained if $\mathbf{c}'$ is the eigenvector corresponding to the smallest eigenvalue of $\mathbf{D}$. Hence, the suboptimal solution in our design problem can be obtained by, first, finding the phases of the eigenvector corresponding to the smallest eigenvalue in $\mathbf{D}$ and then performing a backward linear transformation of the phases by

$$\text{phase of } \mathbf{c} \stackrel{\text{def}}{=} \text{phase of } (\mathbf{U}^{-1} \mathbf{c}') \qquad (18)$$

In this study, the control points are initially set to be edge points of the mainlobe. If the resultant complex filter does not satisfy peak sidelobe conditions, an iterative algorithm is then applied. This iterative algorithm updates the constraint matrix C at each iteration such that the control points are the extrema in the sidelobe region of the previous iteration. The iterative procedure will not terminate until the peak sidelobe constraints are globally satisfied (i.e., all sidelobes are below the threshold). In general, most stable solutions converge at the first iteration.

3 SIMULATION RESULTS

In our simulation, we assume a 1.2 mm diameter array consisting of 256 half wavelength elements operating at 50 MHz with 40 % fractional bandwidth. The broadband response for each focal zone is estimated from point sources located at ranges of 0.8, 1.0, 1.2, 1.4, 1.6, 1.8, 2.0 and 2.2 mm from the origin of the circular array. This simulated rf signal is then baseband demodulated for each of the 256 firings. In order to derive an optimal filter at each range, a representative complex beam pattern (i.e., b), is determined by choosing the complex point for each beam line corresponding to the maximum amplitude along that beam line within a given focal zone. After obtaining the coefficients, this filter is independently applied at each range along the zone. The filter length in all examples is chosen to be 33. This choice is based on the effective angle of acceptance for a circular array, reconstruction complexity and the filter performance. In other words, the imaging aperture consists only of those array elements within 45 degrees of the reconstructed beam direction. One negative consequence of longer filters is that they may produce larger motion artifacts because of the increased data acquisition time. Nevertheless, filter performance is better for longer filters.

In the first example, four elements are tied together per firing. The complex filter coefficients at range 1.4 mm are shown in figure 2, where the top panel shows the amplitude of the filter and the bottom panel shows the unwrapped phase (unwrapped relative to the center of the synthetic aperture). In all figures, *beam index* is defined as the in-
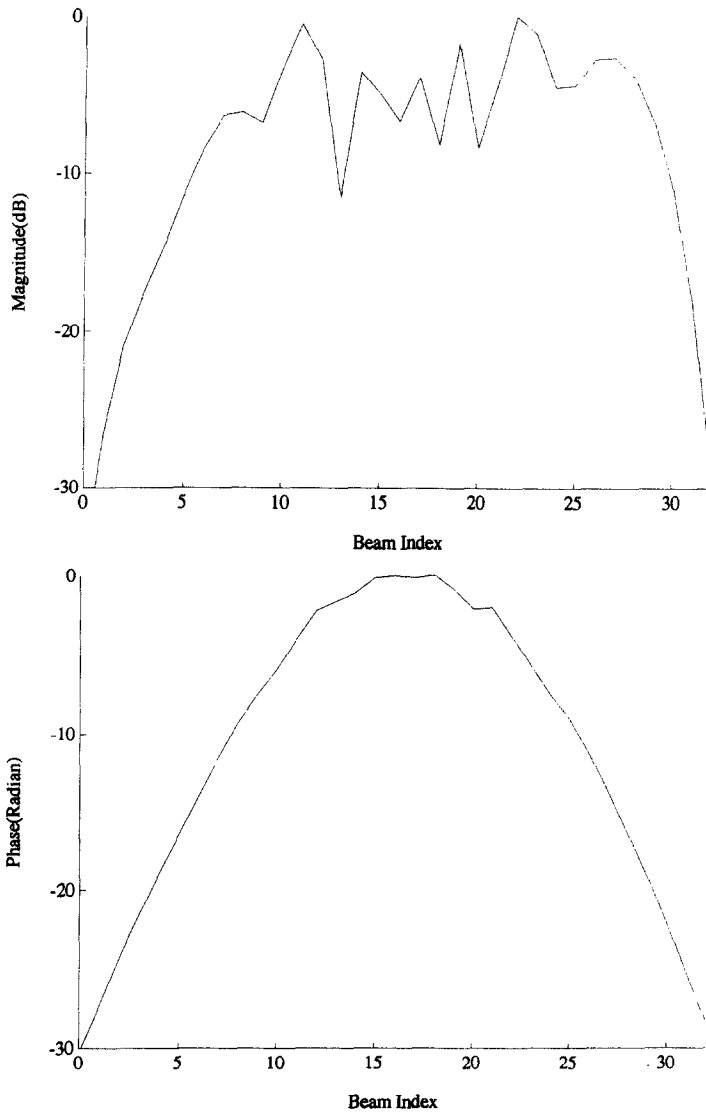
Fig. 2 Complex filter for four element synthetic aperture at range 1.4 mm. The top panel shows the magnitude and the bottom panel the unwrapped phase.

lex for discretized beam angles in the reconstruction plane. Note that the phase of the ilter has a parabolic shape similar to that of a lens. The magnitude, however, is not monotonic and differs significantly from the single element case where the magnitude has a Gaussian shape corresponding to the inverse Fourier transform of an ideal Gaussian beam pattern [9]. Due to the matrix operation in equation(13), coefficients generally are not exactly symmetric about the center of the filter.

In the second example, eight elements are shorted for each firing. The complex filter at a range of 0.8 mm is shown in figure 3. Note that the unwrapped phase shown in the bottom panel does not have a parabolic shape, nor can the magnitude be approximated
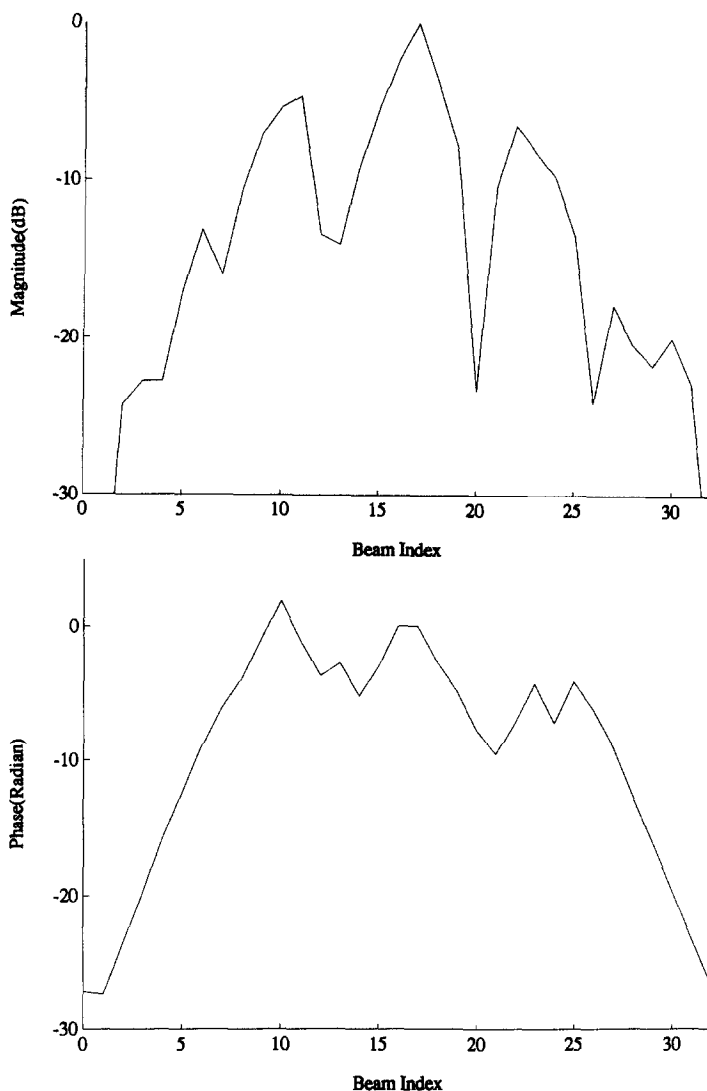
Fig. 3 Complex filter for eight element synthetic aperture at range 0.8 mm. The top panel shows the magnitude and the bottom panel the unwrapped phase.

by a Gaussian function. These filter characteristics result from operating in the near field of the subaperture at this range; therefore, the Fourier transform relationship between aperture function and beam pattern no longer applies. The optimal filter at this near range shows the combined effects of beamforming and decoupling the highly correlated signals between each channel in the subaperture. In contrast, the far field approximation holds at range 1.4 mm, as illustrated by the filter coefficients shown in figure 4. At this range, the magnitude still does not have a simple Gaussian shape since it has to compensate for the narrow angular response of the multi-element subaperture. Again, the top panel of both figures shows the magnitude and the bottom panel shows the unwrapped phase of the filter.
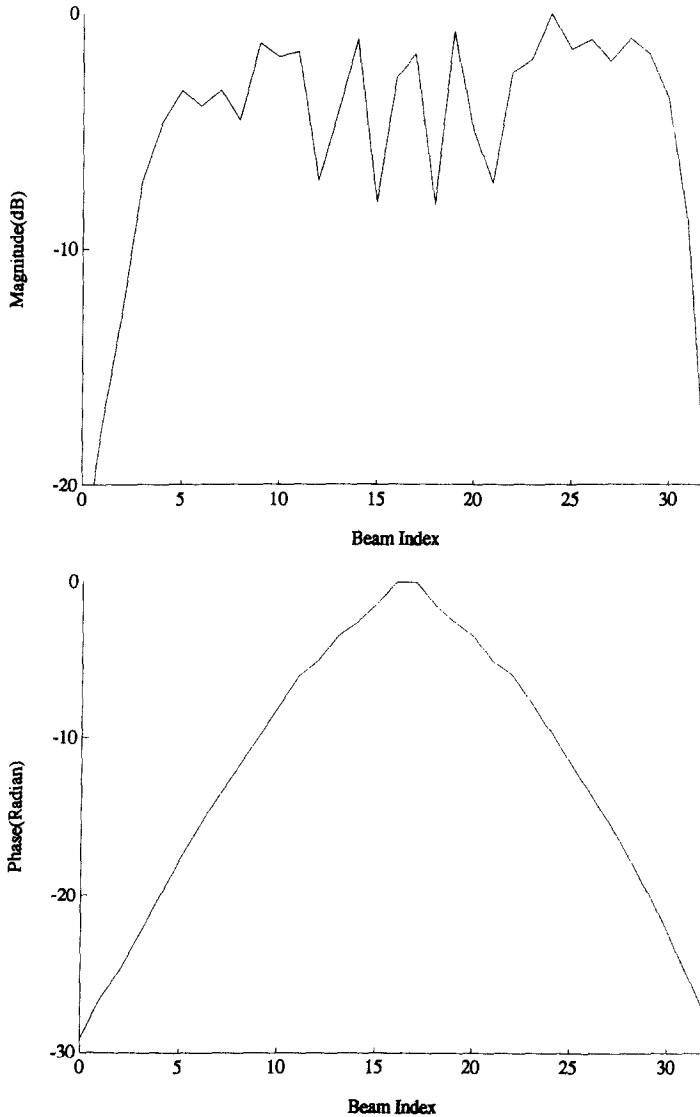
Fig. 4 Complex filter for eight element synthetic aperture at range 1.4 mm. The top panel shows the magnitude and the bottom panel the unwrapped phase.

The broadband response of the circular array is shown in figure 5, where the two left-hand images use four-element synthetic aperture processing and the two right-hand images use eight-element synthetic aperture processing. The top image for each case is the reconstructed output using the Lagrange based filter and the bottom image is the response of the 33 point optimal filter described in Eq. (3). All images are displayed over a 50 dB dynamic range. As we can see from figure 5, the mainlobe beamwidths and the grating lobe levels are about the same for these two filtered outputs. The Lagrange based filter, however, has significantly lower sidelobe levels compared to the original optimal filter especially for four element processing. A final quantitative demonstration of this
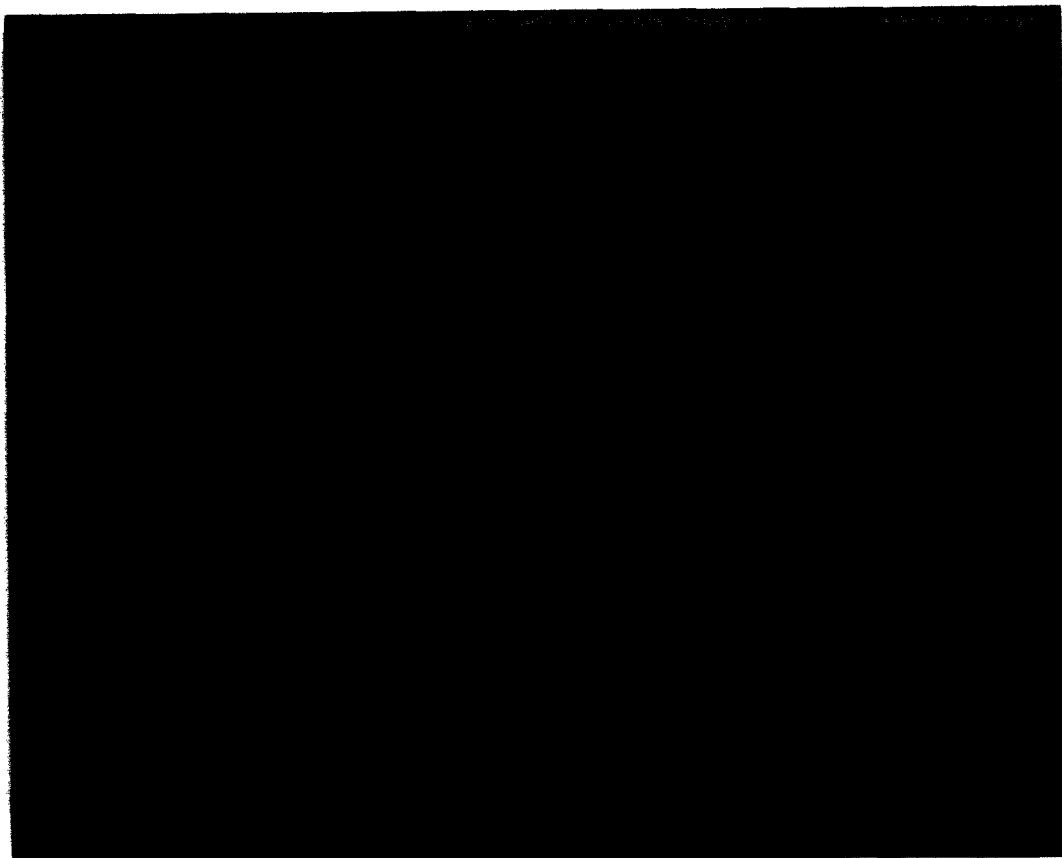
Fig. 5 Reconstructed synthetic aperture images using different filtering approaches. Two top images use four element synthetic aperture processing and two bottom images use eight element synthetic aperture processing. Left hand images are for the Lagrange based filter, whereas right hand images are for the original optimal filter. All images are displayed over a 50 dB dynamic range.

point is presented in figure 6 where beam patterns at a range of 2 mm are presented for the same four cases.

4 DISCUSSION

For single element synthetic aperture processing, complex filtering essentially performs simple focusing with Gaussian apodization. Due to the coupling effect in multi-element synthetic aperture processing, however, the filter tends to compensate for the degraded angular response as well as perform dynamic focusing. Hence, beam pattern and aperture function do not have a Fourier transform relationship and the phase of the filter no longer has simple parabolic shape. This difference is most pronounced in the near field of the multi-element subaperture where the assumption of isotropic insonification used in classic synthetic aperture processing is most violated, as illustrated in figures 2- 4.
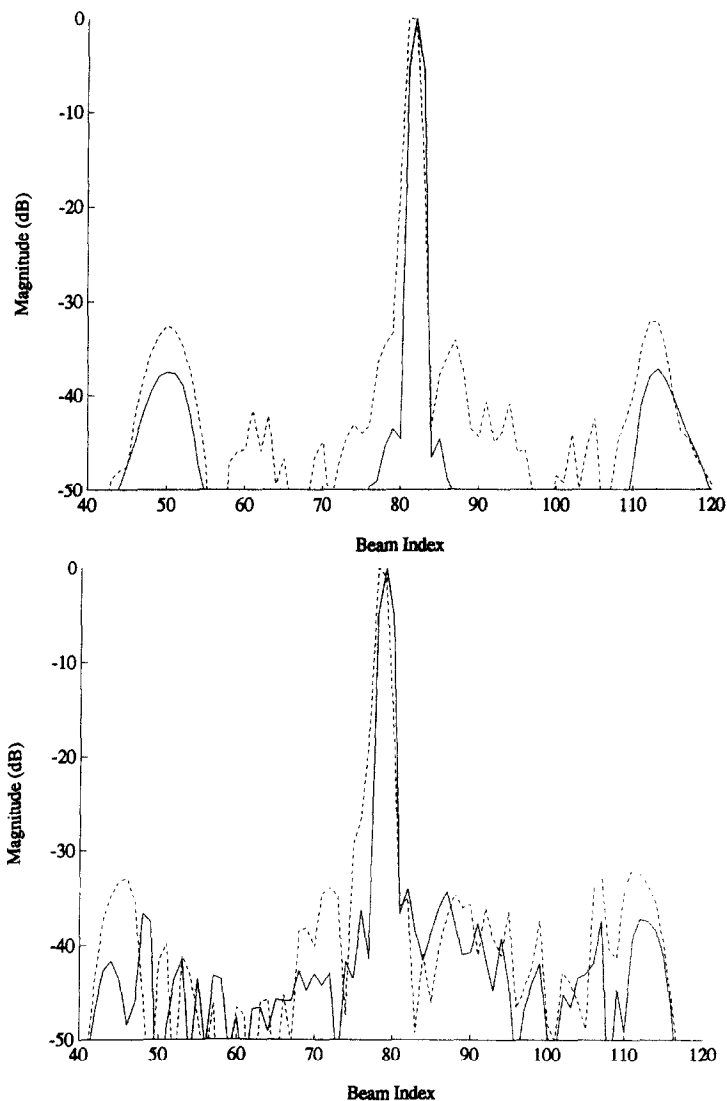
Fig. 6 Beam patterns at range 2 mm. Top panel shows beam patterns for the four element synthetic aperture and bottom panel for the eight element synthetic aperture. Solid lines denote Lagrange based filtering results and dashed lines represent original optimal filtering results in both panels.

A major issue in synthetic aperture reconstruction, as well as all imaging systems, is resolution. Spatial resolution is determined by the energy within the mainlobe region of the reconstructed beam pattern. That is, high level sidelobes will not influence spatial resolution if the sidelobe energy is relatively small. Contrast resolution, however, is more sensitive to sidelobe levels. Consequently, the reduced sidelobe levels of Lagrange based filters offer better contrast resolution without sacrifice of spatial resolution compared to the original optimal filters.

As defined in section 1, multi-element synthetic aperture imaging results in improved electronic SNR compared to classical single element synthetic aperture imaging. The SNR improvement is due to, first, the change in acoustic power delivered to the body from a lower input impedance transducer and, second, different complex filter gains. Using Eq.(1) to analyze the specific filter presented here, SNR gains of about 8 dB were obtained for four or eight element subaperture reconstruction with 33 point filters. This level of SNR improvement is virtually identical to that obtained with the original filter discussed in reference [9]. Consequently, improvements in beam forming with the new filters do not result in reduced electronic SNR compared to the original optimal filters.

Finally, as described in reference [12], we note that our constraint equations in the overall optimization procedure can be changed. However, the problem can no longer be solved by the Lagrange multiplier method. Instead, we will encounter a quadratic programming problem with nonlinear constraints. At this time, it is not known whether complicating the problem in this way will yield better results.

ACKNOWLEDGMENTS

REFERENCES

[1] Pandian, N.G., Intravascular and intracardiac ultrasound imaging: An old concept, now on the road to reality, *Circulation 80*, 1091-1094 (1989).

[2] Yock, P.G. and Linker, D.T., Intravascular ultrasound: Looking below the surface of vascular disease, *Circulation 81*, 1715-1718 (1990).

[3] Bom, N., Lancee, C.T. and van Egmond, F.C., An ultrasonic intracardiac scanner, *Ultrasonics 10*, 72-77 (1972).

[4] Bom, N., ten Hoff, H. , Lancee, C.T., Gussenhoven, W.J. and Bosch J.G., Early and recent intraluminal ultrasound devices, *Int. J. Card. Imaging 4*, 79-88 (1989).

[5] Meyer, C.R., Chiang, E.H., Fechner, K.P., Fitting, D.W., Williams, D.M. and Buda, A.J., Feasibility of high-resolution intravascular ultrasonic imaging catheters, *Radiology 168*, 113-116 (1988).

[6] The entire issue # 4, volume 7 of the journal Echocardiography is devoted to a set of review articles on intravascular and intracardiac ultrasound imaging. Included as the lead article is : Pandian, N.G., Weintraub, A., Schwartz, S.L., Kumar, R., Kusay, B.S., Katz, S.E., Aronovitz, M., Udelson, J., Konstam, M.A., Salem, D.N. and Kreis, A., Intravascular and intracardiac ultrasound imaging: current research and future directions, *Echocardiography 7*, 377-387 (1990).

[7] Schwarz, H.P., Welsch, H.j., Becker, P., Biebinger, M. and Schmitt, R.M., Development of a New Ultrasonic Circular Array for Endoscopic Application in Medicine and NDT, *in Proc. 1988 IEEE Ultrasonics Symposium* 88CH2578-3, 639-642 (1988).

[8] Schwarz, H.P., Welsch, H.J., Becker, P., Biebinger, M. and Schmitt, R.M., Development of a new ultrasonic circular array for endoscopic application in medicine and NDT, *in Proc. 1989 IEEE Ultrasonics Symposium* 89CH2791-2, 687-690 (1989).

[9] O'Donnell, M. and Thomas, L.J. , Efficient Synthetic Aperture Imaging from a Circular Aperture with Possible Application to Catheter-Based Imaging, *IEEE Trans. Ultrason., Ferroelec., and Freq. Contr.*, 39, 366-380 (1992)

[10] O'Donnell, M., Engeler, W.E., Pedicone, J.T., Itani, A.M., Noujaim, S.E., DunkiJacobs, R.J., Leue, W.M., Chalek, C.L., Smith, L.S., Piel, J.E., Harris, R.L., Welles, K.B. and Hinrichs, W.L., Real-Time Phased Array Imaging Using Digital Beam Forming and Autonomous Channel Control, *in Proc. 1990 IEEE Ultrasonics Symposium,* 90CH2938-9, 1499-1502.

[11] Adams, J.W., A new optimal window, *IEEE Trans. on Sig. Proc., 39,* 1753-1769, (1991).

[12] Li, Pai-Chi, Ebbini, E. and O'Donnell, M., A New Filter Design Technique for Coded Excitation Systems, *to appear in November, 1992 issue of IEEE Trans. on Ultrason., Ferroelec., and Freq. Contr.*

[13] Ebbini, Emad, Deep Localized Hyperthermia with Ultrasound Phased Arrays Using the Pseudoinverse Pattern Synthesis Method, Ph.D Dissertation, (University of Illinois, Urbana, IL, 1990).